Performance assessment of multi-tube He II/He II heat exchanger using a single tube sample

Bernard Rousset, F. Millet

Version of Record: https://www.sciencedirect.com/science/article/pii/S0011227522000662
Manuscript_d65f50aa0c4691c2ed4c01bf7b5784de

Performance assessment of multi-tube He II/He II heat exchanger using a single tube sample

B.Rousset*, F.Millet
Univ. Grenoble Alpes, CEA, INAC-SBT, 38000 Grenoble, France
**Corresponding author: bernard.rousset@cea.fr*

Abstract
Superconducting high-field magnets working in He II are usually immersed in a pressurized static He II bath. This pressurized He II bath is then connected through a heat exchanger to a saturated He II bath acting as a cold source. Due to the peculiar He II properties (very high heat conductivity), the conventional heat exchanger designs are not suitable here. Additionally, a compact design is often mandatory, as space inside cryostats is always an issue. In a recent paper [1], we presented different configurations of optimized multi tube heat exchangers depending on the available horizontal or vertical space. Such an optimized compact heat exchanger prototype has been built to fulfill the cooling needs and the integration constraints of the HL-LHC superconducting D2 recombination dipole [2]. The chosen design with hundred oxygen-free high-purity copper horizontal tubes penetrating inside the extremity of the D2 cold mass vessel is an efficient solution offering significant operating margins.
From the thermal analysis, it appears that the profile and value of the temperature difference across the heat exchanger really depends on the ratio of the transverse conductance to the longitudinal conductance, the first being determined by the conductivity of the copper and the Kapitza conductance. Therefore, optimization and prediction of the thermal performance of such a heat exchanger is only possible when these thermal properties (i.e., the heat conductivity and Kapitza conductance of the copper tubes) or the sum of these three thermal resistances in series are well known. For that purpose, we built a dedicated test bench to perform these transverse resistance measurements on a pipe sample. The experimental results obtained on a single pipe were then used to infer the behavior of the complete heat exchanger.
The comparison of the predictive code and the cryogenic measurements shows excellent agreement over a wide range of cryogenic operating conditions (temperatures, pressures, heat loads). This paper presents a guideline for designing compact and efficient He II/He II heat exchanger as well as a method to predict the performance of such heat exchanger accurately.

Keywords: Cryogenics, Superfluid Helium, Heat exchanger, Modelling

Highlights:

- Pressurized superfluid helium thermally linked to a saturated superfluid cold source is commonly used to cool down superconducting devices
- A new approach to design a compact and efficient He II/He II heat exchanger is proposed.
- Experiments fully validate the semi-predictive model.

I - Introduction

To improve magnet cooling and to prevent the risk of film boiling, superconducting high-field magnets working in He II are usually immersed in a pressurized static He II bath. This pressurized He II bath is then connected through a heat exchanger to a saturated He II bath acting as a cold source to remove the heat loads. Due to the peculiar He II properties (very high heat conductivity) and to the heat transfer at wall interface (governed at this very low temperature by the Kapitza resistance

and independent to fluid velocity), the conventional heat exchanger design is not suitable here. In such configuration, convection has no interest for wall heat transfer. The design of the heat exchanger is then reduced to the design of a heat exchanger between two He II baths, one pressurized bath connected to the component (e.g. magnet) to be cooled and the saturated bath used to remove the heat loads.

For a given heat flux to be removed in such multi tube heat exchanger, conduction (including He II heat conduction) imposes a ΔT_{long} increasing with the length L such as $\Delta T_{long} = \alpha.L$. In the opposite, heat exchange through the pipe walls imposes a ΔT_{trans} decreasing with the heat exchange surface which is proportional to the length and therefore $\Delta T_{trans} = \beta/L$. The total ΔT_{tot} is equal to the sum of these two contributions and consequently, $\Delta T_{tot} = \alpha.L + \beta/L$. The general way to solve this kind of problem, i.e. to find the minimum of the ΔT_{tot}, is to find the zero of the derivative of this expression, corresponding here to a minimum selected $L = (\beta/\alpha)^{1/2}$ as illustrated in figure 1. Consequently, the corresponding ΔT_{tot} is then equal to $2.(\alpha.\beta)^{1/2}$ and therefore $\Delta T_{long} = \Delta T_{trans} = \Delta T_{tot}/2 = (\alpha.\beta)^{1/2}$.

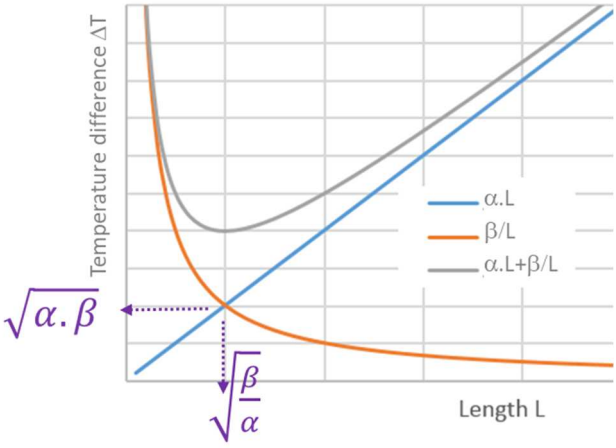

Figure 1 – Pipe length optimization illustration for multi-tube heat exchanger design

It is also important to underline that the calculation of the overall transverse heat coefficient (to assess the β coefficient) needs the knowledge of thermal conductivity of the wall and of the Kapitza conductance on both side of the wall. This latter is very dependent of the material properties and cannot be known accurately without dedicate measurement on a wall sample.

Considering empirical approach, one may think to test heat exchange on a scale down heat exchanger. In case of multi parallel tubes, one possibility is to test separately one pipe, but without a model, this gives no information on the pipe length optimization.

To access this optimization, one needs to couple the measurement of transverse resistance through one pipe sample (performed in a small cryostat) and the use an accurate model (taking into account transverse and longitudinal ΔT through pressurized and saturated He II). This will permit to design the best heat exchanger with the appropriate number and length pipes.

This is why, after recalling previous simplified models in section II, section III introduced temperature gradient both in pressurized and saturated He II, neglecting first the coupling effects. The section IV is dedicated to a more complete code introducing a coupling between longitudinal and transverse heat transfers. Then, section V presents a dedicated measurement of transverse conductance and comparisons between the developed code and the measurements for one single tube heat exchanger and for a multi-tube heat exchanger such as the existing ones illustrated in figure 2.

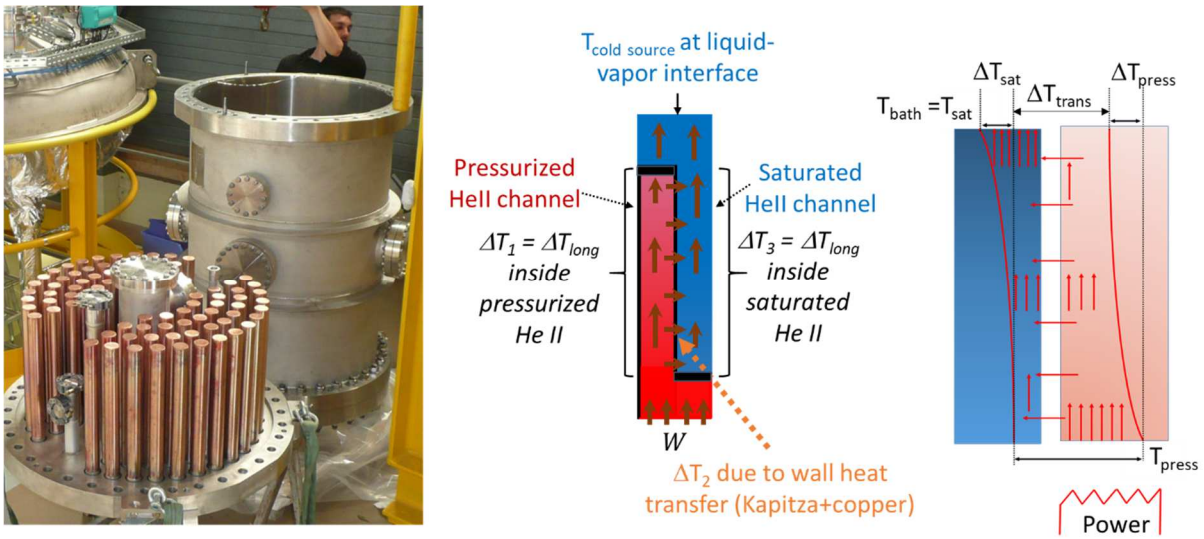

(a)

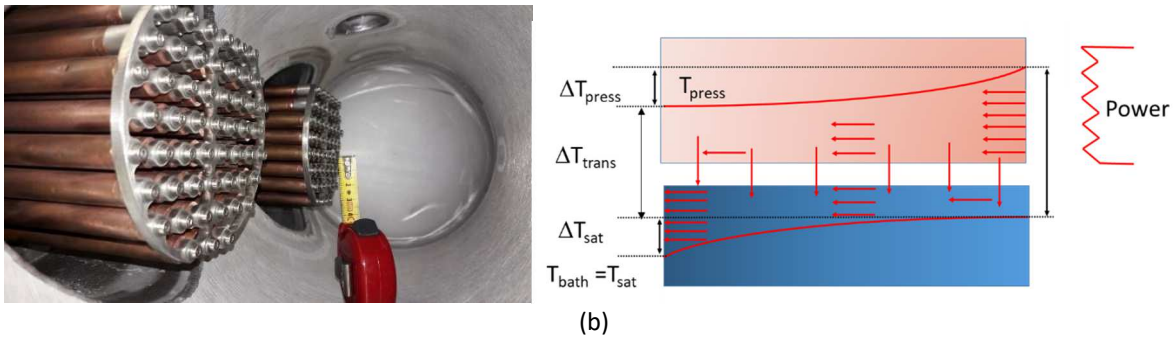

(b)

Figure 2 - Vertical and horizontal multi tube heat exchangers for superfluid helium cooling and corresponding heat transfer and temperature profiles: (a) in turbulence studies [3] at CEA-Grenoble test facility (tube dimensions D42xL400 mm.mm) and (b) in D2 magnets [4] for HL-LHC (tube dimensions D10xL500 mm.mm)

II - Simplified models

The simplest way to design such heat exchanger consists to neglect temperature gradient inside He II baths and to calculate the heat exchange surface A with heat loads, Kapitza conductance and wall conductivity using the following equation.

$$A = \frac{W}{h_{transverse}.\Delta T} = \frac{W}{T_{press}-T_{sat}}\left(\frac{e}{k(\frac{T_{sat}+T_{press}}{2})} + \frac{1}{h_{kap}(T_{sat})} + \frac{1}{h_{kap}(T_{press})}\right) \quad (1)$$

where W corresponds to the power to be removed, T_{press} the temperature of the pressurized He II bath, T_{sat} the temperature of the saturated He II bath as illustrated in figure 2 ($\Delta T_{trans} = \Delta T_2 = T_{press} - T_{sat}$), e the wall thickness, k the wall heat conductivity and h_{kap} the Kapitza resistance. k can be estimated for a given material from literature. It is easy to verify on a sample with electrical measurements (ratio of electrical resistances between 4.2 K and room temperature) as thermal and electrical resistivities of high conductive metals are linked via the Wiedemann-Franz law. The Kapitza resistance h_{kap} is roughly estimated depending on surface material with a typical range from 600 T^3 to 1200 T^3 for copper [5].

This simplified estimate gives the minimum area A required when both saturated and pressurized He II baths are supposed isothermal.

Usually, for practical reasons, He II heat exchangers correspond to one pipe (or a series of pipes in parallel) [3][4][6], with the heat saturated bath inside the pipe(s) and the pressurized He II bath around. However, the cross section corresponding to this (these) pipe(s) may imply longitudinal gradients inside the He II baths.

In his book [7], Steven van Sciver gives a first improvement introducing the longitudinal temperature gradient inside the saturated He II bath only. The pressurized bath linked to the component to be cooled is considered potentially large enough to be isothermal. Such arrangement with one pipe filled with saturated He II is shown on figure 3 and the author provides an analytical solution to solve the corresponding equations.

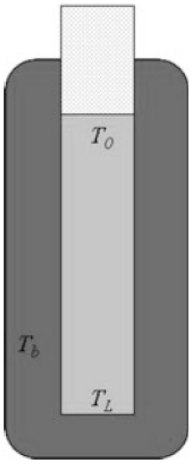

Figure 3 – Schematic view of one pipe He II/He II heat exchanger from [7]

However, this proposed improvement presents some limitations. First, the exponent applied for the Gorter-Mellink relation is fixed to 3 (a former theoretical value) instead of 3.4 (a more recent value) mainly deduced from previous experiments [8][9][10][11][12]. Secondly, the He II pressurized bath temperature (T_b in figure 3) assumed to be uniform, which corresponds to a large pressurized He II cross section, not always available in He II cooling.
Typically, for an external heat exchanger with available space constraints, a limited cross section of the pressurized He II bath has to be envisaged. This is the case of the future D2 recombination dipole of LHC high luminosity upgrade (HL-LHC) as shown on figure 4. To optimize such external heat exchanger, both pressurized and saturated cross section need to be reduced as much as possible.

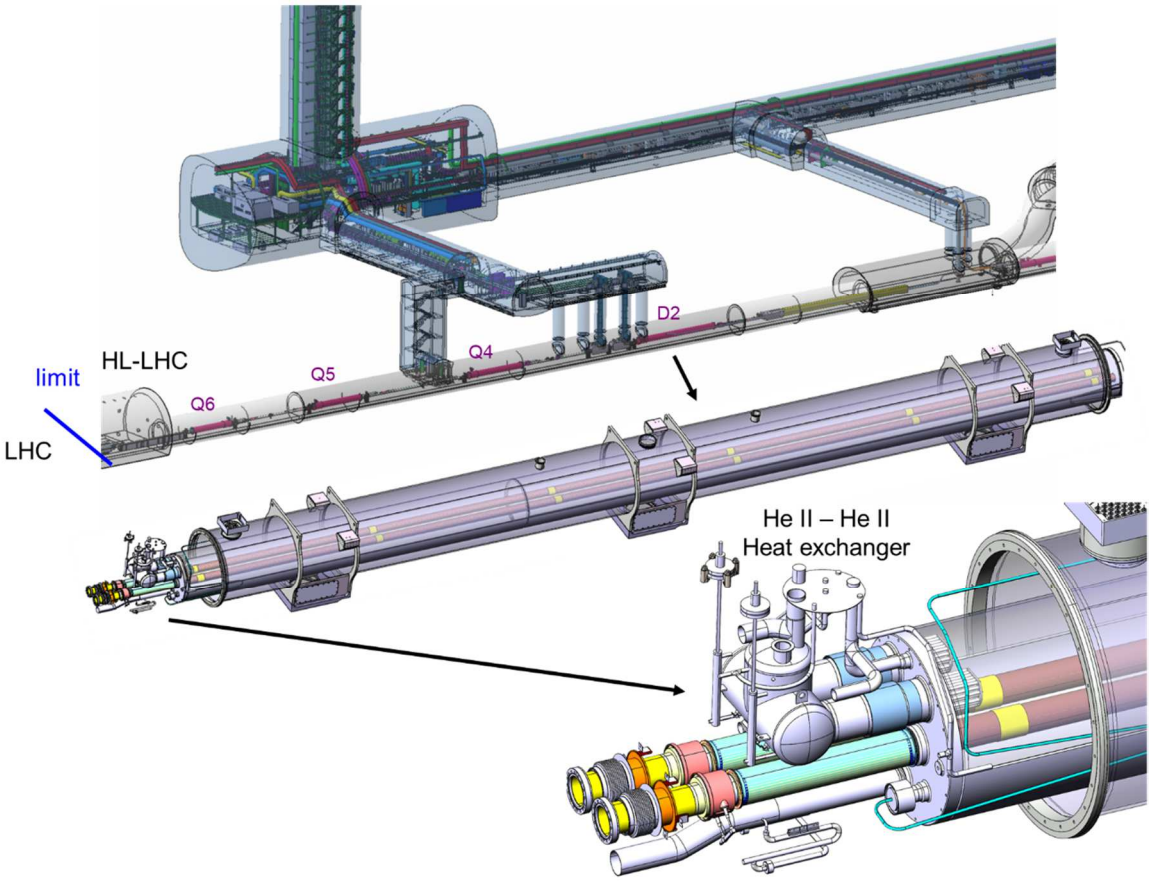

Figure 4 – Integration of a compact He II/He II heat exchanger for the D2 magnets in HL-LHC

III – Uniform transverse heat flux model

A first tentative to optimize the size of such He II/He II heat exchanger has already been published in [1]. The main conclusion was that for an optimized (i.e. minimum) volume, each ΔT (longitudinal ΔT inside pressurized He II, longitudinal ΔT inside saturated He II and transverse ΔT through the wall) should be equal. To reach such conclusion detailed in [1], it imposes the cross section of the pressurized cross section to be equal to the saturated one affected by a ratio of to their apparent conductivity at a power $\frac{1}{3.4}$.

With the requirement of the heat loads to be removed and the specified ΔT_{tot} allowed between the pressurized He II around the magnet and the cold source (saturated He II), the wall exchange surface A is consequently calculated from equation (1) with $\Delta T_{trans} = \frac{\Delta T_{tot}}{2}$, for the optimized pipe length design with $\Delta T_{long} = \Delta T_{trans}$.

The model could be completed to calculate the required cross sections S(P) for saturated and pressurized He II for a given heat exchanger length L. All ΔTs being equal, the transverse heat flux is assumed uniform. Consequently, moving away from the heat source to the cold source, the longitudinal heat flux in the pressurized He II gradually decreases while it gradually increases in the saturated He II.

Practically, under the assumption of uniform transversal heat flux, the corresponding equations for the longitudinal heat flux q are:

$$q_{(x)} = q_0 \frac{x}{L} \quad \text{with} \quad q_0 = \frac{W}{S(P)}$$

Then $$\int_0^L q^{3.4} dx = \int_0^L q_0^{3.4} \frac{x^{3.4}}{L^{3.4}} dx = \frac{q_0^{3.4}}{4.4} L \quad (2)$$

The objective being to link the incoming (or outgoing) transversal heat flux with the longitudinal ΔT, the following heat transport equation for He II is used:

$$\int_0^{\mathrm{L}} \mathrm{q}_{(\mathrm{x})}^{3.4} . \mathrm{dx} = \int_{\mathrm{T}(0)}^{\mathrm{T(L)}} \mathrm{g(T,P)dT} \quad (3)$$

If the ΔTs inside He II are sufficiently small, the apparent heat conduction function $\mathrm{g(T,P)}$ can be assumed uniform and the corresponding equation for the longitudinal ΔT inside He II becomes:

$$\int_0^{\mathrm{L}} \mathrm{q}_{(\mathrm{x})}^{3.4} . \mathrm{dx} \sim \mathrm{g}(\langle \mathrm{T} \rangle, \mathrm{P})\big(\mathrm{T(L)} - \mathrm{T(0)}\big) \quad (4)$$

Then $$\Delta T = T(L) - T(0) = \frac{W^{3.4}.L}{4.4.S^{3.4}\, g(\langle T \rangle, P)} = \frac{\Delta T_{tot}}{2} \quad (5)$$

where the heat flux is evenly distributed with a maximum at x=L equal to q_0 and null for x=0 for pressurized He II while it is the opposite for saturated He II, S(P) is either the pressurized or saturated He II cross section and $g(\langle T \rangle, P)$ corresponds to the apparent heat conduction function at the average temperature $\langle T \rangle$. Note that $g(T,P)$ can be calculated using [12].
One can then deduce the cross section S(P) using the following equation

$$S(P) = \left(\frac{L}{4.4.\frac{\Delta T_{tot}}{2}.g(\langle T \rangle, P)} \right)^{\frac{1}{3.4}} W \quad (6)$$

However, one has to note that this simple calculation does not give access to the temperature profile along the tube but just the temperatures at the extremities. It is also worth mentioning that this approach is only valid for a set of imposed power, temperature and pressure in the pressurized He II bath as the apparent heat conductivity $g(T,P)$ depends both on the temperature and pressure (see figure 5). The temperature dependence being very sensitive, taking the average temperature $\langle T \rangle$ should be considered with an extreme care for $g(T,P)$. It is therefore preferable to apply the integral of the apparent heat conduction function and the equations (2) and (3) become:

$$X_{(T(L),P)} = X_{(T(0),P)} - \frac{q_0^{3.4}}{4.4} L \quad (7)$$

where $X(T,P) = \int_T^{T_\lambda} g(T,P).dT$ as represented on figure 5.
Knowing $q_0,\ T(0),\ P\ and\ L,\ X(T(L),P)$ is calculated and $T(L)$ extracted from the relation between $X(T,P)$ and T.

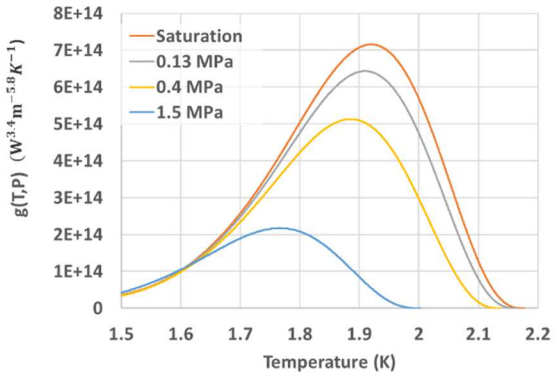

(a) He II apparent heat conduction function

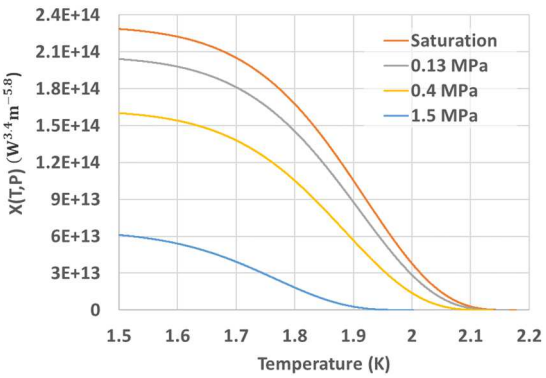

(b) Integral of the He II apparent heat conduction function

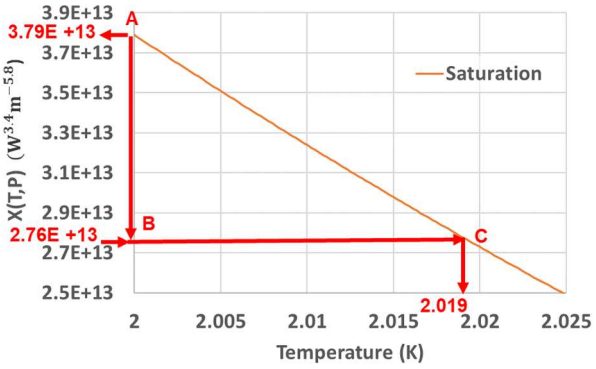

(c) Integral of the He II apparent heat conduction function : example of the numerical evaluation

Figure 5 – Apparent heat conduction function and its integral for superfluid helium

- Numerical evaluation

Configuration with pipes allows 1D calculations inside He II. A numerical evaluation is proposed hereafter for the concrete case to remove 1 W in a single pipe heat exchanger with the saturated He II located inside a 500 mm long single pipe of 10 mm inner diameter (cross section 78.54 mm²) and 1 mm of wall thickness, surrounded by pressurized He II (cross section 121.97 mm²) at 4 bars. We use the value of 3216 W/m²/K (experimental measurement of our pipe sample as described in section V) for the overall transverse heat transfer coefficient (including Kapitza and wall resistances).

At 2 K (cold source), the apparent heat conduction function $g(2\,K, P_{sat}) = 5.69\,10^{14}\,W^{3.4}m^{-5.8}K^{-1}$ and at 2.04 K and 4 bars (maximum conditions for magnet end) $g(2.04\,K, 4\,bars) = 1.59\,10^{14}\,W^{3.4}m^{-5.8}K^{-1}$. As the ratio of the apparent heat conduction function is $\left(\frac{g(2\,K,P_{sat})}{g(2.04\,K,4\,bar)}\right)^{\frac{1}{3.4}} = 1.45$ whereas the cross-section ratio is $\frac{121.97}{78.54} = 1.55$, the thermal gradient along saturated He II should be consequently slightly larger than those inside pressurized He II.

To be conservative, equation (1) is used for the calculation of the transverse ΔT and equation (7) is applied to saturated He II to obtain the longitudinal ΔT_{sat}. Finally, the maximum temperature at the inlet of pressurized He II (magnet side) is then deduced from the calculated ΔT_{sat}. The numerical evaluations are given hereafter:

$$\Delta T_2 = \frac{1}{S_{lateral}\,h_{transverse}} = \frac{1}{0.01571*3216.2} = 0.0198\,K$$

$$X_{(T(L),P_{sat})} = 3.79\,10^{13} - \frac{(1.27\,10^4)^{3.4}}{4.4}0.5 = 2.76\,10^{13}\,W^{3.4}m^{-5.8}$$

$T_{sat}(L) = 2.019\,K$ (see path A-B-C on figure 5c for detail)

$T_{press}(L) = 2.039\,K$

IV – Fully coupled model

To better understand and visualize the limitation of the previous simple model assuming evenly distributed heat flux, a longitudinal meshing of the heat exchanger may be useful.

The solution is to mesh longitudinally the heat exchanger as illustrated in figure 6 and to consider a uniform incoming transverse heat flux to be added (or subtracted for the other channel) to the incoming longitudinal heat flux. We recall hereafter the resulting equations for one channel, those which have been demonstrated by the authors in a previous article [13].

Considering longitudinal heat flux along He II, the proportional repartition has to be changed to a linear repartition including an offset, as heat flux coming from the previous mesh element must be added. The corresponding equation (details in [13]) becomes:

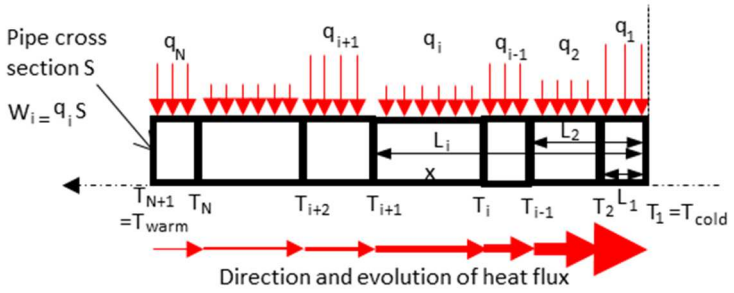

Figure 6 – Heat load distribution example in He II – He II heat exchanger

$$X_{(T(L_i),P)} = X_{(T(L_{i-1}),P)} - \frac{\Sigma_i^{4.4}}{22 q_i}(L_i - L_{i-1})\left(\left(-\frac{q_i}{\Sigma_i}+1\right)^{\frac{2}{5}}.\left(5\left(\frac{q_i}{\Sigma_i}\right)^4 + 20\left(\frac{-q_i}{\Sigma_i}\right)^3 + 30\left(\frac{q_i}{\Sigma_i}\right)^2 - 20\frac{q_i}{\Sigma_i}+5\right)-5\right) \quad (8)$$

with $$\Sigma_i = \sum_{j=i}^{N} q_j$$

For each mesh element, the solution is obtained in a same way as in previous section with equation (8) replacing equation (6). This set of equations is numerically applied to the same conditions as previously in section III.

The results are presented on figures 7a and 7b showing the temperature profiles along the saturated and pressurized He II channels as well as the evenly distributed heat flux used in the calculations.

The boundaries conditions are taken at 500 mm for the saturated He II (cold source temperature fixed at 2 K in the following example) and at 0 mm for the pressurized He II (magnet end temperature) by adding the constant transverse ΔT to the saturated He II temperature calculated previously.

As foreseen, the temperature at extremities (2 K, 2.019 K and 2.039 K) are equal to those given by the model using linear heat flux distribution without discretization. However, the temperature profiles are not parallel and consequently the transverse heat flux cannot be evenly distributed.

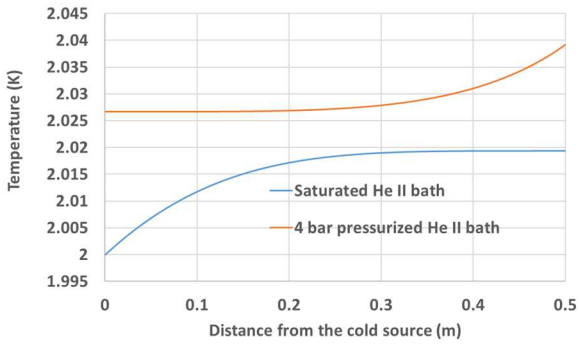

Figure 7a - Temperature profile with the outlet saturated He II temperature imposed at 2 K (simple calculation without any coupling).

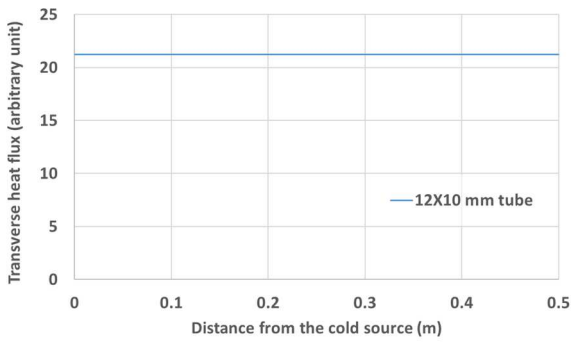

Figure 7b - Uniform transverse heat flux used to calculate independently the temperature profiles inside saturated He II, pressurized He II

Looking in more detail to the temperature profile, it appears clearly that removing (or adding) a constant value of heat flux correspond to a larger temperature gradient when the total longitudinal heat flux is large, which is due to the power law response of heat flux versus temperature.

Consequently, we can observe a large decrease in temperature for pressurized He II at the inlet of the channel (where heat flux inside pressurized He II is at maximum) and a large decrease for saturated He II at the opposite extremity where all the heat flux has been transferred.

Obviously, when temperature gradient are larger, the transverse heat flux is larger too (as $q_{t(i)}=h_{transverse}S_{lateral(i)}(T_{HeIIpress(i)}-T_{HeIIsat(i)})$ which is in contradiction with the hypothesis of uniform transverse heat flux shown in figure 7b. Consequently, it will modify the temperature profiles inside the He II channels.

To solve this coupled problem, we use an iterative process described on the flow chart presented on figure 8.

This initialization process consists first to calculate the longitudinal temperature profile along the saturated he II pipe assuming an evenly distributed transverse heat flux. So longitudinal heat flux decreases linearly from the inlet to the outlet whereas the temperature increase with inlet temperature corresponding to the temperature at the liquid-vapor interface. As the refrigerator will impose this inlet temperature, the calculation will proceed from this inlet of tube where the temperature is minimum and heat flux maximum to the inlet where the heat flux is zero but the temperature is maximum. This first calculation gives the saturated He II temperature profile for a uniform transverse heat flux. Always assuming uniform transverse heat flux, the temperature difference between pressurized and saturated He II is calculated at each mesh element introducing the overall heat transverse coefficient.

At that stage, the loop can begin with a coupled calculation. The inlet pressurized He II temperature (latest mesh node as the inlet is at the opposite extremity of the cold source, i.e. point 3 on the plots figure 8) is calculated by adding the temperature difference coming from transverse heat flux calculation at previous step. The pressurized temperature profile is calculated from the inlet to the outlet by subtracting the heat flux going to the saturated He II.

The next step consists of recalculating the transverse heat flux with the difference of the pressurized and the saturated temperature profiles. The new total transverse heat flux (sum of transverse heat flux for individual mesh element) is compared to the power injected and rescaled if needed to compensate any difference. If the ratio is close to one, then the calculation has converged. If not, the new transverse heat flow (after re-scaling) is introduced for the next calculation of saturated and pressurized temperature profiles. This results in a new temperature difference and finally a new transverse heat flow. It generally converges after a few steps (< 10).

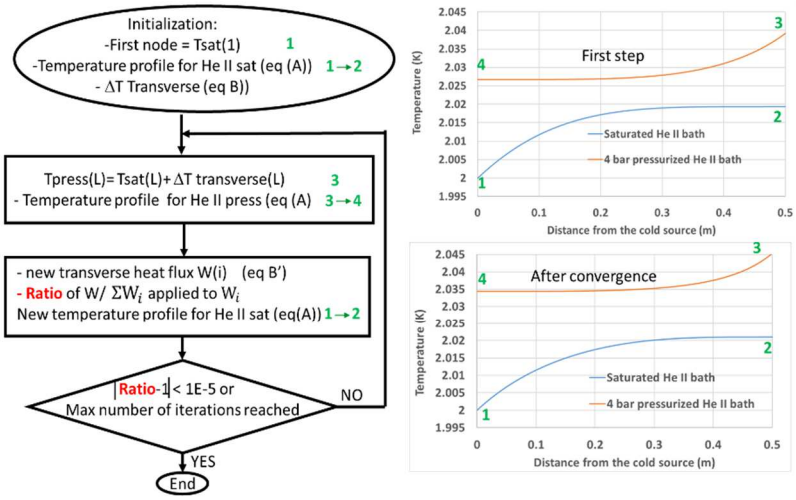

$$X_{(T(L_i),P)} = X_{(T(L_{i-1}),P)} - \frac{\Sigma_i^{4.4}}{22 q_i}(L_i - L_{i-1})\left(\left(-\frac{q_i}{\Sigma_i}+1\right)^{\frac{2}{5}} \cdot \left(5\left(\frac{q_i}{\Sigma_i}\right)^4 + 20\left(\frac{-q_i}{\Sigma_i}\right)^3 + 30\left(\frac{q_i}{\Sigma_i}\right)^2 - 20\frac{q_i}{\Sigma_i} + 5\right) - 5\right) \quad \text{eq A}$$

$$\Delta T2(i) = \frac{W(i)}{S_{lateral}\, h_{transverse}} \quad \text{eq B} \qquad W(i) = S_{lateral}\, h_{transverse}\, \Delta T2(i) \quad \text{eq B'}$$

Figure 8 – Iterative process for coupled problem in He II – He II heat exchanger

Applying this to the previous conditions, new temperature profiles and transverse heat flux are calculated and presented on figures 9a and 9b. Maximum temperature (inlet of the pressurized He II channel) is equal to 2.045 K, instead of 2.039 K, i.e. an overall increase of ΔT larger than 15 % (45 mK versus 39 mK).

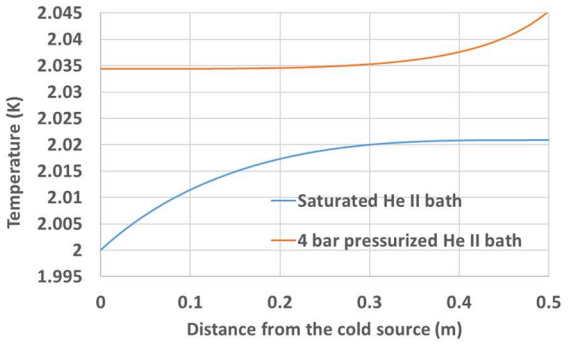

Figure 9a - Temperature profile with outlet saturated He II temperature imposed at 2 K (results obtained with complete model)

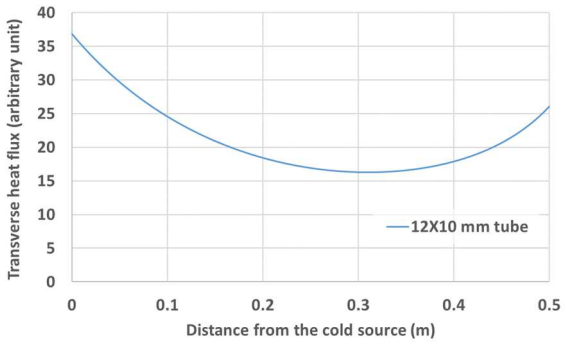

Figure 9b - Real transverse heat flow resulting from the coupling.

Obviously, the same code can be applied with another set of parameters (total power to be removed, cold source temperature or other heat exchanger geometric dimensions).

It is worth mentioning that this coupled calculation does not depend on a specific ratio between pressurized He II and saturated He II cross sections, and the code can be used also far from the "optimized volume" heat exchanger.

In some case, the power (heat flow) may not come from the extremity of the pressurized He II channel but may be evenly distributed or the pressurized He II bath may be very large so the He II temperature inside can be considered as uniform. In this latter case, we recover the case already treated by van Sciver [7], however using the power 3.4 for the flux instead of 3. Furthermore, use of numerical integration is in any case needed to access the detail of the temperature profile along the saturated channel.

V - Experimental facilities and validation of model

Three different set-ups are used to fully characterize a multi copper pipe heat exchanger and to validate entirely the developed model. Two set-ups use a laboratory cryostat to measure a single copper pipe channel performances as illustrated in figure 10.

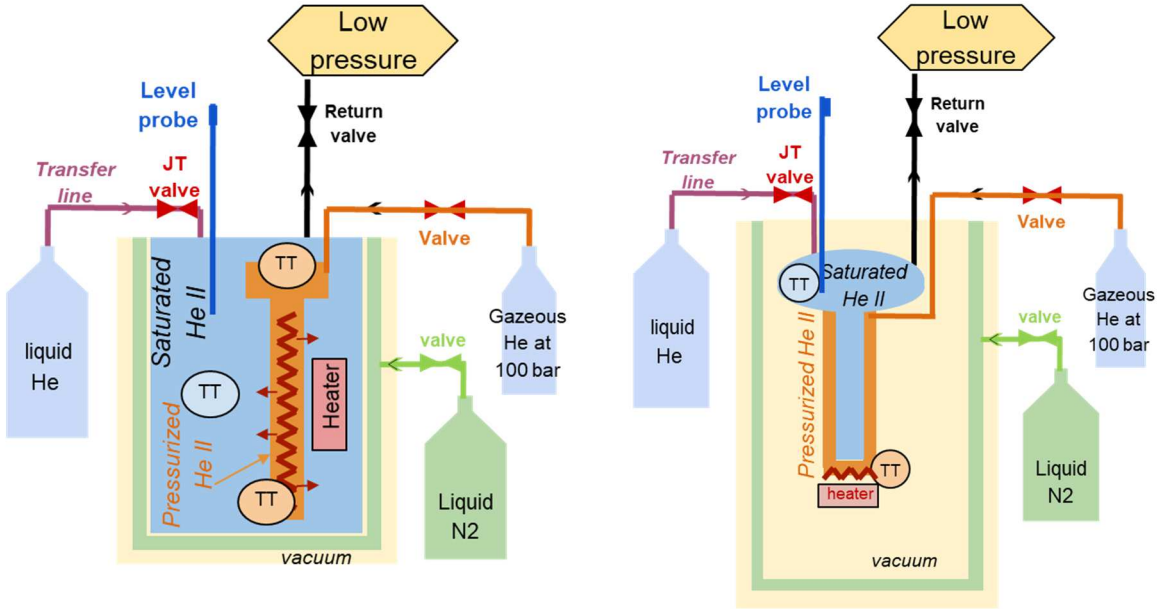

(a) Transverse heat transfer coefficient measurements

(b) Single pipe heat exchange performance measurements

Figure 10 – One pipe heat exchanger characterization in two testing configurations

The third one requires the 1.8 K test facility at CEA-Grenoble to assess the performances of the heat exchanger prototype built for the D2 magnets at CERN in the framework of the HL-LHC [4].

V.I - Test bench to measure transverse heat transfer coefficient on a pipe

The first set-up is dedicated to the overall transverse heat transfer coefficient measurement. This coefficient corresponds to three thermal resistances in series, namely Kapitza resistance between pressurized He II and wall, wall thermal resistance and Kapitza resistance between wall and saturated He II. To impose an uniform heat flux through the pipe wall, we need to have perpendicular heat flux lines. To do so, we choose to introduce the pressurized He II inside the pipe, and the saturated He II bath outside (see figure 9a). With a very large saturated bath, we can ensure an uniform saturated He II bath temperature. Then we introduce inside the pipe a heater deposited on a sheet of kapton. The heater occupies the whole length of the pipe, so the power is evenly distributed inside the pressurized channel. This geometrical arrangement allows an uniform heat flux normal to the pipe wall. To verify this, two thermometers (one at the bottom and another at the top) are introduced inside the pipe, and a third thermometer is installed inside the saturated bath. All cryogenic temperature sensors are Cernox®. The thermometers are fixed with fiberglass supports and are fully surrounded by liquid helium during the measurements. We verify that the temperature increase at the top and the bottom of the pressurized He II bath are equal for each value of the injected power, which fully verify the absence of longitudinal gradient when injected power is applied.

We also minimize parasitic heat load (mainly associated with superfluid critical heat flux) coming from room temperature by using a long capillary pipe to connect the pressurized He II to the room gas supply. Furthermore, this connection to the heat exchanger tube is located at its top, so the heat flux does not have to cross over the tube before being removed. As a consequence, the parasitic heat

load has poor influence in the overall transverse heat coefficient measurement, as it result only in a small offset on ΔT, which can be removed considering that ΔT is zero for zero power injected.

A gaseous helium (GHe) sub-atmospheric pumping system is used to remove the injected heating power (0 to 1 W) and to actively regulate the He II saturated bath at the required temperature. We performed three series of tests corresponding to three saturated bath temperatures of 1.62, 1.8 and 1.99 K. For each temperature, different heating powers are applied with either increasing or decreasing values to measure the steady state regime and to verify the absence of any hysteretic effect.

For all temperatures, the two thermometers inside pressurized He II have identical behavior as illustrated in figure 11 with temperature difference between the pressurized and saturated He II baths at the two thermometer positions. Furthermore, figure 11 shows small change in temperature and a simple linear fit (instead of a more complex power law) can be used to describe the transverse heat transfer coefficient dependence with temperature as illustrated in figure 11d.

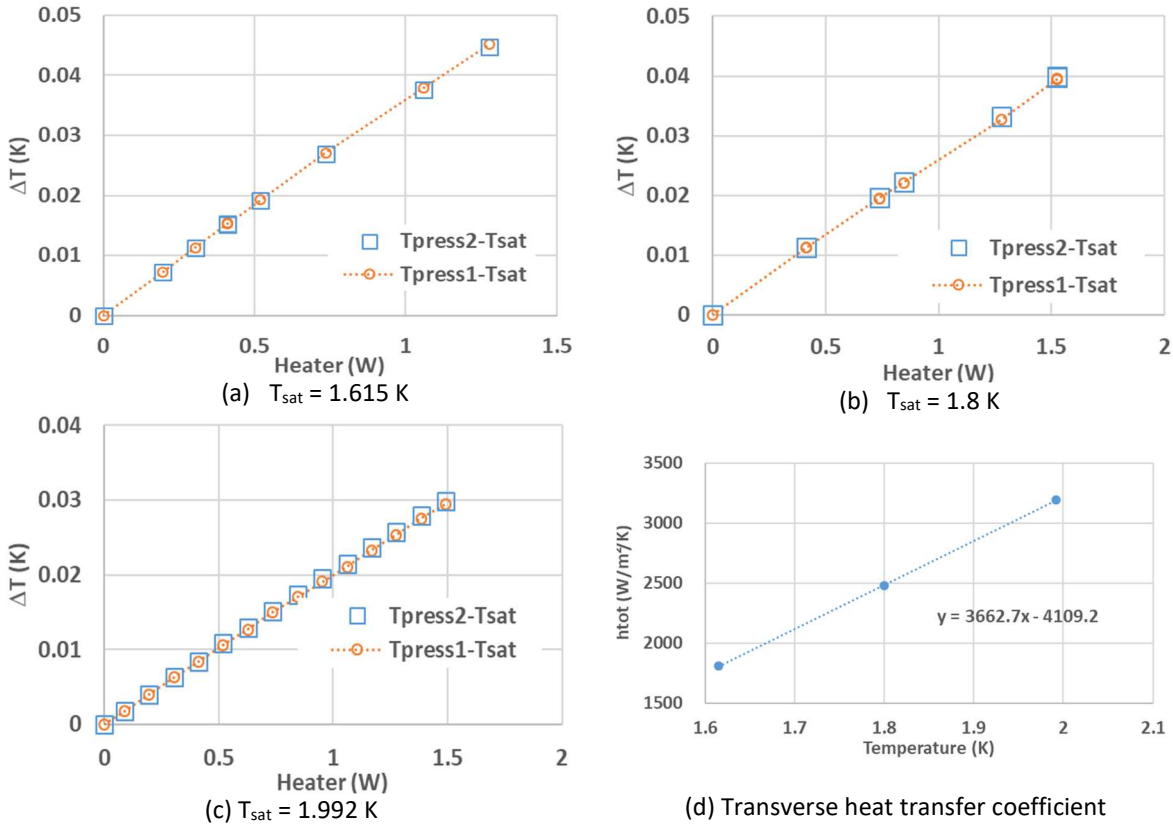

(a) T_{sat} = 1.615 K

(b) T_{sat} = 1.8 K

(c) T_{sat} = 1.992 K

(d) Transverse heat transfer coefficient

Figure 11 – Experimental results for transverse heat transfer characterization of one copper pipe

V.II - Test bench to validate the heat exchange performance on a single pipe

The knowledge of the transverse heat transfer coefficient should be sufficient to use the code previously described in a predictive way. To verify this, we use the previous heat exchanger tube sample in a configuration identical to its final application. The previous setup configuration is modified accordingly as illustrated in figure 10b. That time, the heat exchanger pipe is filled with saturated He II and a larger stainless steel pipe filled with pressurized He II is placed around the pipe. The annular cross section between the two pipes is designed to offer a similar geometrical configuration to the real multi tube heat exchanger. At the bottom of this annular cross section, a

local heater simulates the heat load (0 to 1 W) to be extracted, whereas at the top, a capillary pipe is necessary to fill with pressurized He II.

As in the previous configuration, a GHe sub-atmospheric pumping system is used to remove the injected heating power and to actively regulate the saturated He II bath at the required temperature (1.8 K or 2 K).

Classically, the test cryostat has to limit the static heat loads and multi-layer insulation (MLI) is installed on all cold surfaces to limit thermal radiation and a high-vacuum pumping system actively pumps the test cryostat enclosure to limit the conduction and convection heat leaks in the test apparatus.

This is particularly important as the temperature gradient along He II is not proportional to the heat flux but obeys to a power law. Therefore, fixed parasitic heat losses cannot be considered as an offset as its influence increases when the total heat flux increases. Consequently, the parasitic heat losses should to be as low as possible with a residual part estimated with maximum accuracy.

Unfortunately, when no additional load is injected in our test cryostat, the measured temperature difference given by thermometers inside pressurized and saturated He II still give a value (either positive or negative) corresponding to the sum of thermometer inaccuracy and heat losses. For instance, with no injected power, the temperature inside pressurized He II is lower by roughly 1 mK than the saturated bath temperature, whereas we estimate the heat losses to 0.1 W, corresponding to a temperature difference of 2.5 mK according to our fully coupled model. Consequently, for the comparison between the model and the tests, we systematically apply an offset of 3.5 mK on all temperature difference measurements and an additional heat of 0.1 W to experimental injected power.

The experiments are performed for two saturated bath temperatures (1.8 K and 2 K) and two pressures for pressurized He II in the annular cross section (1.3 bar and 4 bar). The valve on the gaseous helium pumping regulates the saturated He II bath temperature at a setting value within typically 0.1 mK, for temperature ranging from 1.8 to 2 K and various mass flow corresponding from 0 to 1 W of injected power. Measurements are taken once the required temperature is reached and with decreasing liquid level inside the saturated He II bath to avoid additional loss potentially coming from the transfer line. We stop the measurements as soon as the liquid level inside the saturated He II bath is too close to the top extremity of the heat exchanger tube. We then re-open the liquid helium transfer line to fill again the saturated He II bath for a new run.

The performed series of tests allow us to assess the performances of one single pipe heat exchanger and to verify the accuracy of the semi-predictive model using the measured values of heat conductivity and Kapitza conductance issued from the previous tests and the He II heat transport properties from literature. Figure 12 presents the comparison of the experimental results with the advanced model predictions for two temperatures. The heat transverse measurements coming from the previous configuration are also reported in the same figure.

The predictions given by the model are in very good agreement with the experiments, with surprisingly lower discrepancy than one should except for such difficult measurements.

During the tests, we observe some instabilities for some experimental points, especially at 1.3 bar. Indeed, after being filled, cooled and set at the required pressure, the pressurized He II bath is closed, and has a volume at low temperature and another one at room temperature close to the supply valve installed at room temperature. Any change of temperature inside this closed volume

due to power injection or vapor flow along the long capillary pipe, induces pressure variations and it can be tricky to control them, especially for large injected powers. Nevertheless, it appears obvious that the pressurized He II temperature increase is higher at 4 bar than at 1.3 bar for the same high injected power as shown in figure 12. This is mainly due to the very close proximity of superfluid/normal fluid transition. When the pressure increases, the transition temperature decreases. In addition, for high-injected power, the heat conductivity function is much lower for 4 bar than for 1.3 bar close to temperatures at lambda transition at 4 bar as illustrated in figure 5.

Considering the model application, we also experiment some divergence of the code close to the lambda transition. This is due to the very sharp variation of $X_{(T,P)}$ coming from very large values of order of 10^{13} close to zero. Of course, for concrete applications of heat exchanger design, nobody wants to work so close to the lambda transition and the model works perfectly in such conditions far enough from the lambda transition vicinity.

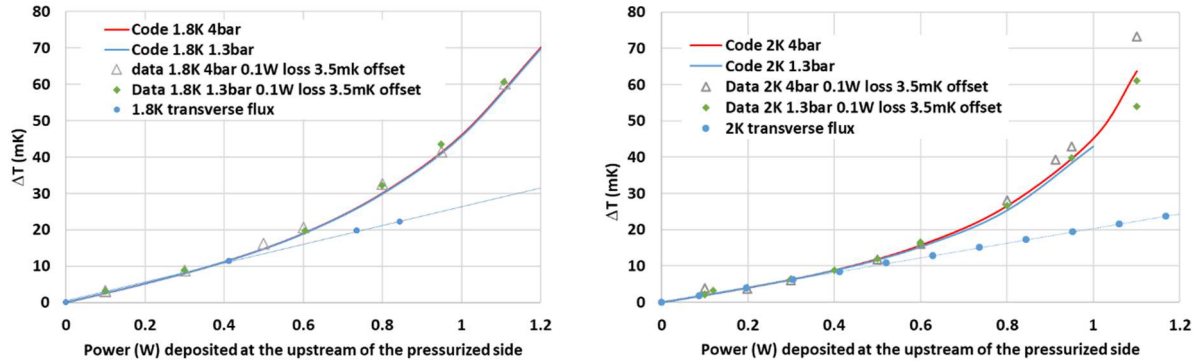

(a) T_{sat} = 1.8 K (b) T_{sat} = 2 K

Figure 12 – Experimental results for a single copper pipe He II/He II heat exchanger

V.III - Use of the 400W@1.8K test facility to validate a prototype of heat exchanger for HX-D2

The last test consists of validating the thermal behavior of a complete multi tube heat exchanger. CEA DSBT shall provide such He II/He II heat exchangers in a framework of the HL-LHC project and a prototype has been designed and tested prior to the series manufacturing.

The design of the heat exchanger prototype has been already described in [1] and the achieved performances presented in [4]. As shown in figure 13, the heat exchanger prototype consists of hundred horizontal copper tubes in parallel connecting a saturated He II bath (cold source) with a pressurized He II enclosure simulating the D2 magnet operating conditions. The cold source design for the liquid-vapor interface provides sufficient hydrostatic pressurization of the saturated He II in the copper tubes to prevent any risk of film boiling even for the highest heat flux to be removed.

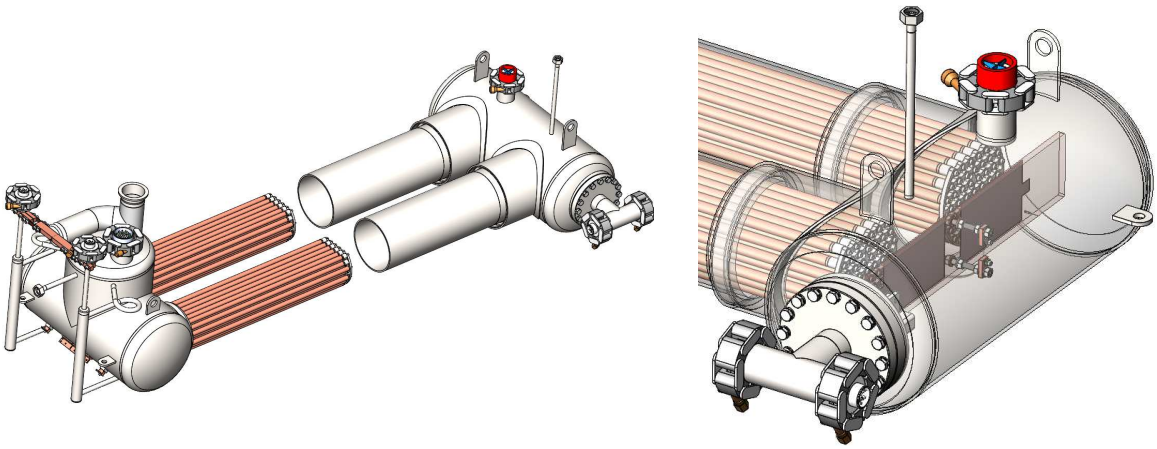

Figure 13 – 3D views of a compact HeII/HeII heat exchanger for the D2 magnets in HL-LHC

Various experimental runs permit measurements at different bath temperatures and gives an estimation of heat losses at 5.5 W and uncertainties in temperature difference measurements between the pressurized and saturated He II baths lower than 0.5 mK as reported in [14].

The real dimensions of the heat exchanger prototype are introduced in the advanced model to predict its performances and compare them to experiments taking into account the heat losses. It is worth mentioning that the cross sections ratio of pressurized and saturated He II in the prototype is set at 2.039 to mimic the D2 magnet design. This value is therefore larger than the tested one in the single pipe test configuration (set at 1.55). This ratio difference is due to surrounding areas around the multi-tube arrangements.

Figure 14 presents the comparison of the experimental results and the prediction of the advanced model at 1.8 and 2 K. We also add on the same figure the transverse heat flux extrapolation (multiplication of single tube heat exchange by 104, the tube number) of the previous measurements performed for the single pipe heat exchanger (first configuration).

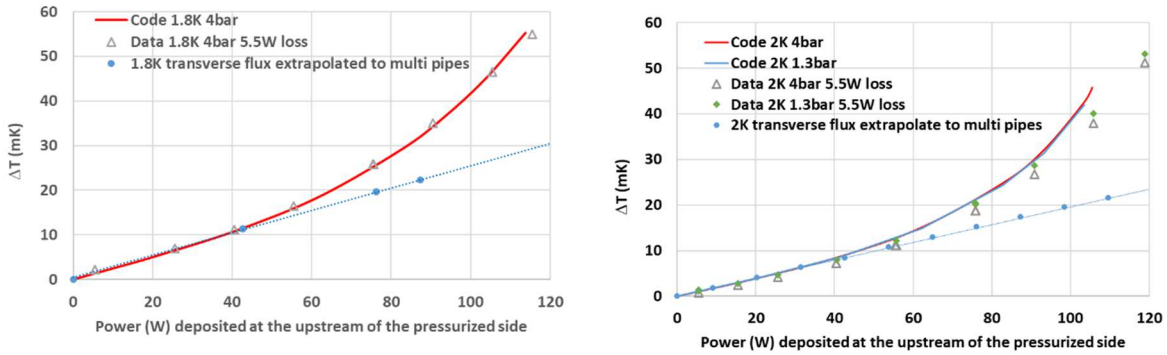

(a) T_{sat} = 1.8 K (b) T_{sat} = 2 K

Figure 14 – Comparison of experimental results and model for the multi-tube prototype

At 1.8 K, the agreement between the code and the measured data is practically perfect and the discrepancy is substantially lower than the sum of all uncertainties. One can also see the quasi-linear behavior at low heat flux where the transverse thermal resistance is predominant and a transition to a power law at higher heat flux where the longitudinal ΔT due to temperature gradient inside He II becomes important.

At 2 K, even if the agreement between the experiments and the model is still very good, small discrepancies are visible at large heat fluxes. The code gives a higher ΔT, which may be due to the

non-exact estimation of the longitudinal ΔT inside the pressurized side of the heat exchanger. Indeed, to reproduce the real condition of installation inside the D2 magnet, the final part of the heat exchanger has a larger cross section at the inlet of the test cell as observable in figure 13, as it will be inserted inside the magnet cryostat. This is negligible for the thermal behavior, except close to the lambda line where helium heat conductivity vanishes. This may explain why the experimental data gives a lower ΔT close to the lambda transition.

VI - Conclusion

Even if He II cooling is currently used in scientific research infrastructures, a method to design an optimized He II/He II heat exchanger is still lacking. To address this issue, we propose a methodologic approach for the design of an efficient and compact He II/He II multi-tube heat exchanger.

Assuming a periodic arrangement of the tubes inside the heat exchanger, the problem is reduced to one “period”, i.e. one pipe filled internally with saturated He II (or pressurized He II) surrounded by the proportional equivalent cross section filled with pressurized He II (or respectively saturated He II). Taking into account an optimized (minimum) volume and a global ΔT specification for the heat exchanger, the cross sections for pressurized and saturated He II are calculated. With a simple model, the heat exchanger is calculated using a simple analytical solution without coupling between temperature gradient along pressurized and saturated He II. With such assumption, the calculations allow a first prediction with an accuracy of a few percent depending on the working temperature. For a more accurate model applicable independently of the pressurized/saturated He II cross section ratio, a complete coupling and a discretization of the pipe length are mandatory. This advanced model is described and compared with experiments at different working temperatures and input powers. The agreement between model and experimental data is satisfactory within the sensor accuracy (i.e. usually better than 1 mK for the total ΔT between each extremity of the heat exchanger).

To run the code efficiently, the boundaries conditions are of the first importance. It first concerns the heat exchanger geometry (pipe length and cross sections for pressurized and saturated He II). Secondly, the transport and transfer properties are important too. The transport properties for He II are now well known based on [12] and the use of the integral of the apparent heat conduction function offers an efficient way to solve the equation of heat inside He II. In the opposite, accurate data is more difficult to obtain for the transfer properties (i.e. wall heat conductivity and Kapitza resistance at the wall-He II interfaces). The wall heat conductivity really depends on the material (purity of copper for instance as well as it state (annealed or not)) and the Kapitza resistances may vary on a large range depending on the material surface (roughness, oxidation…). For rough estimates, the designer can use figures reported in the material bibliography. For a more accurate design, the authors suggest, as presented in the paper, to perform a dedicated measurement of the overall heat transverse coefficient (sum of the Kapitza and wall thermal resistances) on a tube sample among the bench of the tubes for the heat exchanger.

Following the procedure described in this paper, the design of an efficient and compact He II/ He II heat exchanger is now accessible.

Acknowledgments

This work is partially performed in the Framework Collaboration Agreement KN3573/GEN between CERN and CEA and its Addendum n°3 KE5016 for the production of superfluid helium heat exchangers for the stand-alone magnets D2 for the High Luminosity upgrade for the LHC. The authors

would like to thank the CEA colleagues, Lauriane Martinet, Pierre Nivelon, Thomas Goy, Michel Bon-Mardion, Julien Inigo, for the support during the heat exchanger measurements.

References

[1]. Rousset B *et al.* Superfluid Helium cooling and compact Heat Exchanger for HL-LHC D2 Recombination Dipoles*, 2019 IOP Conf. Ser.: Mater. Sci. Eng.* **502** 012114

[2]. Fabbricatore P, Bersani A, Caiffi B, Cereseto R, Farinon S, Foussat A, et al. Development of a Short Model of the Superconducting Separation Dipoles D2 for the High Luminosity Upgrade of LHC. IEEE Trans Appl Supercond 2018;28:1–5. doi:10.1109/TASC.2017.2772779.

[3]. Rousset B et al., Superfluid High REynolds von Karman experiment, Rev. Sci. Instrum. **85**, 103908 (2014).

[4]. Rousset B *et al. Cryogenic performances of a heat exchanger prototype suitable for the superconducting HL-LHC recombination dipole D2, IOP Conference Series: Materials Science and Engineering, Advances in Cryogenic Engineering from CEC-2021 to be published*

[5]. Camacho D, Chevassus S., Policella C., Rieubland JM., Vandoni G., van Weelderen R. Thermal Characterization of the HeII LHC Heat Exchanger Tube, 17th International Cryogenic Engineering Conference, Bournemouth, UK, 1998, pp.647-650

[6]. Claudet G, Aymar R. Tore Supra and He II Cooling of Large High Field Magnets. In: Fast RW, editor. Advances in Cryogenic Engineering: Part A & B, Boston, MA: Springer US; 1990, https://doi.org/10.1007/978-1-4613-0639-9_8

[7]. Van Sciver SW. Helium Cryogenics. New York, NY: Springer New York; 2012. doi:10.1007/978-1-4419-9979-5.

[8]. Bon Mardion G., Claudet G., Seyfert P., Practical data on steady state heat transport in superfluid helium at atmospheric pressure, Cryogenics, Volume **19**, Issue 1, 1979, Pages 45-47, ISSN 0011-2275, https://doi.org/10.1016/0011-2275(79)90109-7

[9]. Kashani A., Van Sciver S.W., High heat flux Kapitza conductance of technical copper with several different surface preparations, Cryogenics, Volume **25**, Issue 5, 1985, Pages 238-242, ISSN 0011-2275, https://doi.org/10.1016/0011-2275(85)90202-4.

[10]. Iwamoto A., Maekawa R., Mito T., Kapitza conductance of an oxidized copper surface in saturated He II, Cryogenics, Volume **41**, Issues 5–6, 2001, Pages 367-371, ISSN 0011-2275, https://doi.org/10.1016/S0011-2275(01)00082-0.

[11]. Darve C., Huang Y., Nicol T.H. and Peterson T.J., "Experimental investigations of He II heat transfer through a short section of LHC inner triplet quadrupole heat exchanger," in *IEEE Transactions on Applied Superconductivity*, vol. **11**, no. 1, pp. 1629-1632, March 2001, doi: 10.1109/77.920092.

[12]. Sato A, Maeda M., Kamioka Y., Chapter 201 - Normalized representation for steady state heat transport in a channel containing He II covering pressure range up to 1.5 MPa, Editor(s): Liang Zhang, Liangzhen Lin, Guobang Chen, Proceedings of the Twentieth International Cryogenic Engineering Conference (ICEC20), Elsevier Science, 2005, Pages 849-852, ISBN 9780080445595, https://doi.org/10.1016/B978-008044559-5/50204-0.

[13]. Rousset B, Millet F. Evaluation of Superfluid Helium Cooling Schemes and Application for HL-LHC Recombination Dipole D2. Cryogenics 2018, https://doi.org/10.1016/j.cryogenics.2018.08.004

[14]. Rousset B *et al.* Assessment of the operation safety margin of the HL-LHC superconducting recombination Dipole D2 in case of helium filling failure*, IOP Conference Series: Materials Science and Engineering, Advances in Cryogenic Engineering from CEC-2021 to be published*